Met. Mater. Int., Vol. 21, No. 3 (2015), pp. 498~503
doi: 10.1007/s12540-015-4433-7

Effect of Zr Thin Film on Zr Foil as a FCCI Barrier Between Lanthanide (La-Ce) and Clad Material

Kang Soo Lee[1,2], In Yea Kim[2], Wooyoung Lee[1,*], and Young Soo Yoon[2,*]

[1]Department of Materials Science and Engineering, Yonsei University, Shinchondong, 262 Seongsanno, Seodaemoongu, Seoul 120-749, Republic of Korea
[2]Department of Environment and energy engineering, Gachon University, Seongnamdaero 1342, Gyeonggi-do 461-710, Republic of Korea

(received date: 18 September 2014 / accepted date: 12 December 2014)

Zirconium (Zr), a potential candidate for preventing Fuel-Cladding Chemical Interaction, shows stable inter-diffusion behavior between cladding and fuel materials. However, a 25 μm-thick Zr foil allows local inter-diffusion, due to defects generated during manufacturing. In this study, we investigate the use of a Zr thin film deposited on Zr foil for preventing local inter-diffusion. The diffusion behavior of the Zr thin film on Zr foil was investigated using misch metal (Ce: 75% and La: 25%) as fuel fission product, in order to effectively simulate nuclear fuel. While without the Zr barrier substantial inter-diffusion occurred at the interface between the ferritic/martensitic HT9 cladding material and misch metal, the Zr thin film on Zr foil exhibited excellent resistance to inter-diffusion. The enhancement of the barrier ability of the Zr thin film on Zr foil was attributed to a lower amount of defects induced by the Zr thin film layer.

Keywords: diffusion, intermetallics, vapor deposition, scanning electron microscopy (SEM), FCCI barrier

1. INTRODUCTION

The sodium-cooled Fast Reactor (SFR) has been highly acclaimed as next-generation nuclear reactor due to its good performance in recycling nuclear spent fuel by pyroprocessing. Moreover, U-Zr metal fuel shows better performances in a nuclear reactor than other nuclear fuel types. The U-Zr metal fuel has advantages such as easy manufacturing of the fuel rod, excellent compatibility with sodium, proliferation resistance, and thermal conductivity [1]. However, inter-diffusion occurs between actinide elements (fission products from the nuclear fuel) and the surfaces of cladding at the operating temperatures of the SFR. This phenomenon, labeled FCCI, is also responsible for the formation of lower melting point eutectic phases [2-6]. The thickness of the cladding is gradually reduced during the nuclear reactor operation, in such a case, steadily decreasing the mechanical strength of the cladding. In particular, intermetallic reactions between cerium lanthanide fission products and cladding produce brittle compounds like Fe_2Ce [7]. Many barrier studies have attempted to prevent the FCCI, for instance through metallic foils and coating [8-12]. Diffusion barrier of FCCI is required to deposit thin layer in order to maintain good thermal conductivity and provide less defect in the thin barrier. The film deposited by R.F sputtering has advantages of high deposition rate and good uniformity in the atomic scale even on large-area substrates compared with pulsed laser deposition, chemical vapor deposition, and thermal evaporation. Among several candidates, a Zr foil or Zr thin film fabricated using physical and chemical vapor deposition on the cladding showed good performance in reducing the FCCI [2-13]. On the other hand, steels such a Fe, Fe-Cr, D9, and HT9 used as cladding have been assessed by out-of-pile tests with diffusion couples in order to investigate the FCCI behavior of metallic fuel alloys [14-17]. Because HT9 and T91 ferritic/martensitic steels exhibit excellent irradiation resistance, they have been considered as potential candidates for SFRs cladding [18].

Jee *et al*. have synthesized Zr thin film as FCCI barrier at various temperatures using hydrothermal crystallization. Although Zr thin films prevented inter-diffusion of the misch metal, the process was not entirely avoided [19]. Yang *et al*. have investigated electroplating of a ~20 μm-thick Cr barrier in order to define inter-diffusion behavior depending on the crack size in the Cr diffusion barrier. The inter-diffusion was effectively interrupted by the plated Cr layer at bath temperature of 353 K which has shallow crack [11]. However, the Cr barrier contained more number of defect and deep crack of Cr barrier at at bath temperature of 740 K which induced inter-diffusion. It implies that diffusion properties is considerably depending

*Corresponding author: benedicto@gachon.ac.kr, wooyoung@yonsei.ac.kr

on size and number of defect. In our case, the structural integrity of Zr thin film/Zr foil appears much more effective at obstructing inter-diffusion compared to other systems.

In this study, we propose the deposition of a Zr thin film on Zr foil by radio frequency magnetron sputtering as a route to reduce the number of defects in the Zr metal foil, that represent the diffusion pathway from nuclear fuel to cladding. The diffusion barrier for various specimens, such as: 1) mish metal vs. HT9, 2) mish metal vs. 25 μm Zr foil, and 3) mish metal vs. Zr thin film deposited on 25 μm Zr foil, was evaluated by out-of-pile diffusion couple tests between HT9 and misch metal as fission product. The Zr thin film on Zr foil specimen showed better performance for limiting inter-diffusion because the dense and homogeneous Zr thin film filled out local defect sites in the Zr film, effectively preventing inter-diffusion of the misch metal.

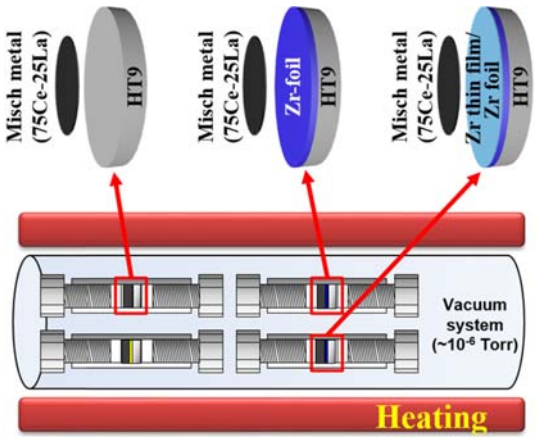

Fig. 1. Schematic illustration of the diffusion specimens in a vacuum furnace.

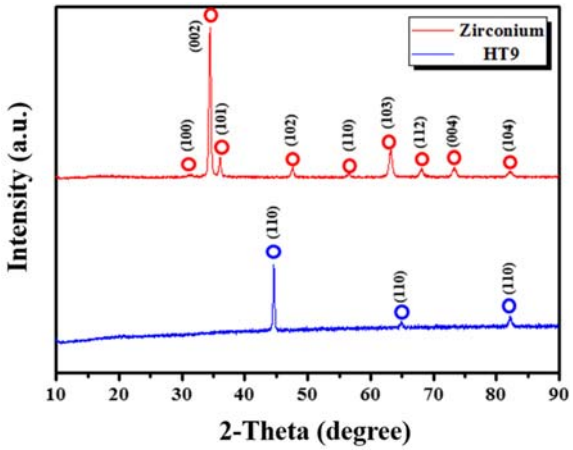

Fig. 2. XRD spectra of Zr foil and HT9 as barrier and cladding material respectively.

2. EXPERIMENTAL PROCEDURES

2.1. Material and preparation

Ferritic/martensitic HT9 steel disks were used to conduct diffusion couple tests. The diameter and thickness of the polished HT9 disks were 7 and 2 mm, respectively. Table 1 shows the specific composition of HT9. The HT9 disks were polished with fine silicon carbide paper for minimizing the surface roughness factor. Before the deposition of the Zr thin film, a 25 μm Zr foil (Alfa Aesar Co., Inc., 99.8% purity) was cleaned by ultra-sonication in acetone and isopropyl alcohol for 15 min. The Zr thin film was deposited on the Zr foil at 100 W for 5 hour under base and working pressures of 4.0×10^{-4} Pa and 6.5×10^{-1} Pa, respectively. A chromium thin film was deposited as glue layer at 20 W for 15 min on the Zr foil substrates, in order to enhance adhesion between the Zr thin film and the Zr foil. The substrate holder was rotated at a speed of 40 rpm in order to minimize the biased growth of the deposition layer.

2.2. Diffusion couple test

The diffusion couple test was carried out to investigate the FCCI reaction between cladding material and a rare earth element as fission product at the operation temperature of an SFR. Natural misch metal consist mainly of La: 25% and Ce 75%, which was probably to be a good candidate for simulation of the inter-diffusion behavior between rare earth and cladding materials. The prepared specimens were inserted into a 316 stainless steel screw jig as shown in Fig. 1, and then firmly tightened. In order to prevent reaction with the 316 stainless steel jig, the specimens were covered with tantalum foil (thickness 0.25 mm, ≥99.9%, Aldrich). After clamping, the sample was put into a vacuum furnace for 24 h at 933 K under a pressure of 5.3×10^{-3} Pa. The above temperature was chosen based on the general operation temperature of an SFR. After completion of the diffusion couple test, the specimens were subjected to air cooling.

2.3. Sample characterization

X-ray diffraction (XRD, Rigaku RINT) was used to investigate the crystal structures of the Zr foil and HT9 specimens. To investigate the structure and the phases present, the Zr specimen was prepared for transmission electron microscopy (TEM) using a Focused Ion Beam (FIB) instrument (FEI Co. NOVA 200, Eindhoven, Netherlands), as shown in Fig. 3. The FIB source was equipped with Ga ion at 30 kV. The crystal structures of each specimen were investigated by X-ray dif-

Table 1. Chemical composition (wt%) of the HT9 steel

Steel	Fe	Cr	Ni	C	W	Mo	Si	V	Other
HT9	84.36	11.94	0.62	0.21	0.48	1.03	0.69	0.30	0.37

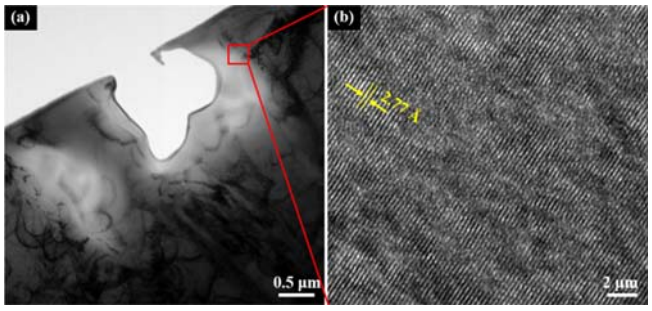

Fig. 3. TEM images of Zr foil (a) using FIB technic and (b) at high - resolution.

fraction (XRD, Rigaku RINT) and high-resolution TEM (HR-TEM, JEM-2100F, JEOL). The specimens were cut vertically to characterize inter-diffusion using a field emission scanning electron microscope (FE-SEM, Hitachi S-4200). The thickness and surface of the Zr thin film and foil were examined by FE-SEM. The elemental distribution after the diffusion couple test were determined by line Energy Dispersive Spectrometry (line EDS).

3. RESULTS AND DISCUSSION

3.1. Characterization of materials

The crystalline structure of the samples was determined by XRD. Figure 2 shows the XRD patterns of the as-deposited Zr foil and HT9. The peaks of Zr foil can be clearly seen in the diffraction patterns, corresponding to crystal systems of hexagonal structure (JCPDS, No. 65-3366), as shown in Fig. 2. On the other hand, HT9 induced three peaks that can be indexed to a cubic chromium ion phase (JCPDS, No. 65-7775).

Figure 3(a) shows the TEM image of the FIB specimen at low magnification. A HR-TEM image of a typical Zr metal is shown in Fig. 3(b). Periodic lattice fringes were observed across the Zr foil. The measured lattice spacing is 2.77Å, corresponding to the (100) plane of zirconium. The *d* spacing is 2.79Å for the (100) plane, according to JCPDS No. 65-3366.

The Zr thin film and foil were analyzed by FE-SEM. Figure 4(a) and (b) show surface and cross-sectional images of the Zr thin film as FCCI barrier. The Zr thin film exhibited columnar microstructures perpendicular to the Cr/silicon substrate. The specimen has compact, flat surfaces without defects such as pinholes and voids. Compact and flat surfaces disrupt inter-diffusion by reducing the diffusion pathways. On the other hand, Figure 4(c) shows the presence of many cracks and trenches on the surface of Zr foil, which provide diffusion sites for the FCCI phenomenon. In the present study, we deposited Zr thin film on the surface of the Zr foil for preventing inter-diffusion, according to the role of Zr foil defects in the FCCI process. The Zr foil covered with Zr thin film shows dense and smooth surfaces, similar to the surface of Zr thin film on silicon wafer shown in Fig. 4(a).

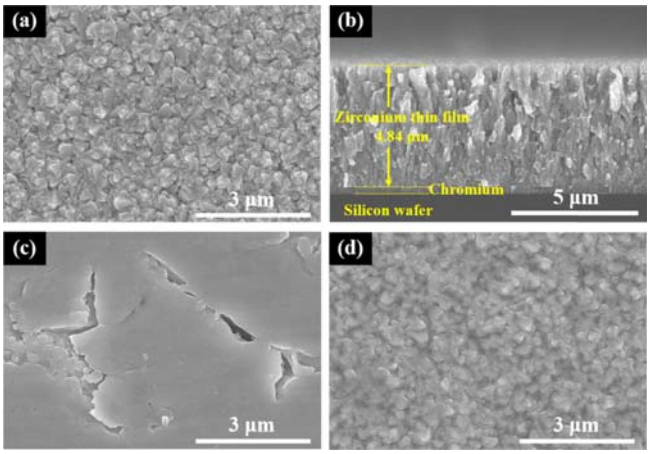

Fig. 4. FE-SEM images of (a) surface of Zr thin film, (b) cross section of Zr thin film, (c) surface of Zr foil, and (d) surface of Zr foil after Zr thin film deposition.

3.2. Reaction between misch metal and HT9

The microstructure of the specimens after the diffusion couple test at 933 K is shown in Fig. 5, 6, and 7. Figure 5

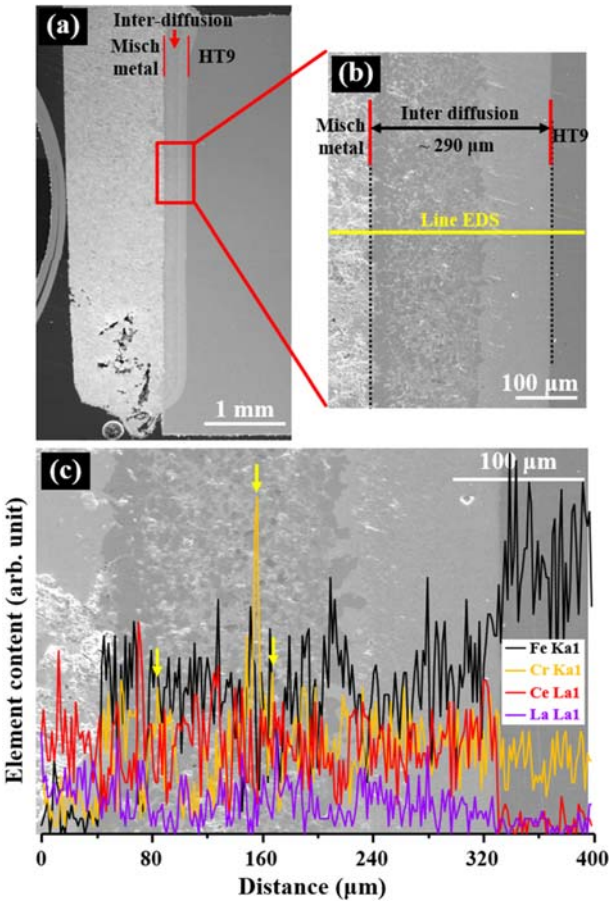

Fig. 5. FE-SEM images of the misch metal/HT9 specimen after diffusion couple test. (a) at low magnification (40x), (b) enlarged image from the (a), and (c) EDS line profiles for elements content at magnification (300x).

shows a cross-sectional FE-SEM image of misch metal with HT9. The low magnification (40x) image in Fig. 5(a) clearly confirms that heavy inter-diffusion at all over HT9 was induced at the SFR operation temperature of 933 K. The thickness of the inter diffusion layer, as shown in Fig. 5(b), was ~290 μm, confirming that accelerated simulation of the FCCI reaction between nuclear fuel and cladding was effectively achieved. Figure 5(c) shows the elemental content of the diffusion-coupled misch metal/HT9 specimen. Fluctuations in the Ce content were observed going from the misch metal to the interface. Moreover, the Ce content rapidly decreased at the end of the inter-diffusion line near the clad at 323 μm, which can be distinguished by FE-SEM. Fe was also detected as an intermediate phase near to the misch metal, as shown in Fig. 5(c). In the inter-diffusion region (~290 μm) on the HT9 side, substantial precipitation near the misch metal/HT9 interface was induced by the diffusion couple test (indicated by an arrow in Fig. 5(c)). The analysis of the precipitation by SEM/EDS reveals a Cr-rich phase: as it can also be seen from the Ce-Cr phase diagram, Cr cannot dissolve in the Ce matrix at 933 K [20].

Figure 6 shows the cross-sectional image of the misch metal/25 μm-thick Zr foil/HT9 specimen at low magnification (40x). Although the Zr foil effectively prevented inter-diffusion across each interface compared with the misch metal/HT9 specimen, localized inter-diffusion was observed at 933 K, as shown in Fig. 6(a). This phenomenon occurred through bulk defects in the Zr foil surface, as illustrated in Fig. 6(c). The localized inter-diffusion length shown in Fig. 6(b) is ~286 μm, similar to the corresponding length in misch metal/HT9 (see Fig. 5(b)), for which localized defects in the Zr diffusion barrier seriously affected inter diffusion at the SFR operating temperature. The EDS elemental line profiles of the misch metal/Zr foil/HT9 specimen are shown in Fig. 6(c). The Fe atoms of HT9 penetrated the Zr foil via the defects. Concurrently, the Ce atoms of misch metal also diffused across the interface. On the other hand, La barely diffused into the HT9, indicating that the La atoms diffused less than the Ce ones and reacted with the steel.

The microstructure of the misch metal/Zr thin film/Zr foil/

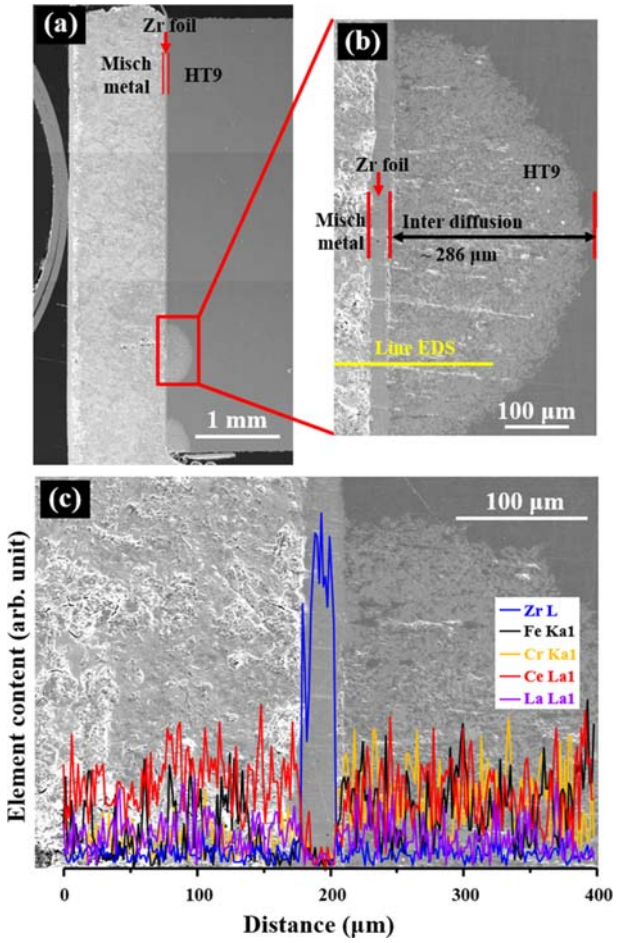

Fig. 6. Effect of the FCCI barrier of misch metal/Zr foil/HT9 specimen after diffusion couple test. (a) at low magnification (40x), (b) Enlarged image of localized inter diffusion from (a), and (c) EDS line profiles for elements content with Zr foil barrier at 300x magnification.

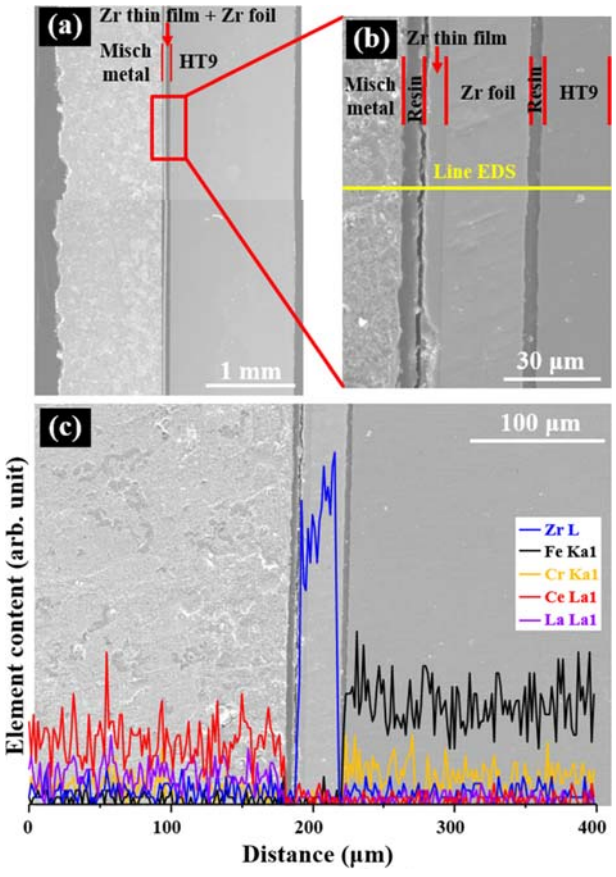

Fig. 7. Effect of the FCCI barrier of misch metal/Zr thin film/Zr foil/HT9 specimen after diffusion couple test. (a) at low magnification (40x), (b) enlarged image at 1500x magnification from the (a), and (d) EDS line profiles for elements content at 300x magnification.

HT9 specimen after the diffusion couple test at 40x magnification (Fig. 7(a)) shows no clear evidences of inter-diffusion and Cr precipitation. Position of EDS line profile was confirmed by Fig. 7(b). The Zr thin film layer was homogeneously deposited on the Zr foil. The misch metal/Zr thin film/Zr foil/HT9 sample was observed at 1500x magnification (Fig. 7(b)) in order to examine it thoroughly. The image highlights distinct individual interfaces, showing that the Zr thin film/Zr foil acts effectively to prevent inter-diffusion. Resin as gray region at the interface between misch metal and Zr thin film/Zr foil or Zr thin film/Zr foil and HT9 was confirmed as shown in Fig. 7. The presence of resin means there are obviously no diffusion of the each contents. However, in case of inter-diffusion at the interface (see Fig. 5, and 6), resin was not observed because each contents was chemically diffused over the interface and there are no space for permeating resin. This is also confirmed by the EDS line profile, as shown in Fig. 7(c). Fe and Cr from HT9 cannot penetrate into the Zr thin film/Zr foil than also no observation of Cr precipitation. Even though, as mentioned above, Ce easily diffused into the HT9 matrix, in the present case Ce was obviously blocked due to the dense and defect-free Zr thin film/Zr foil hybrid structure.

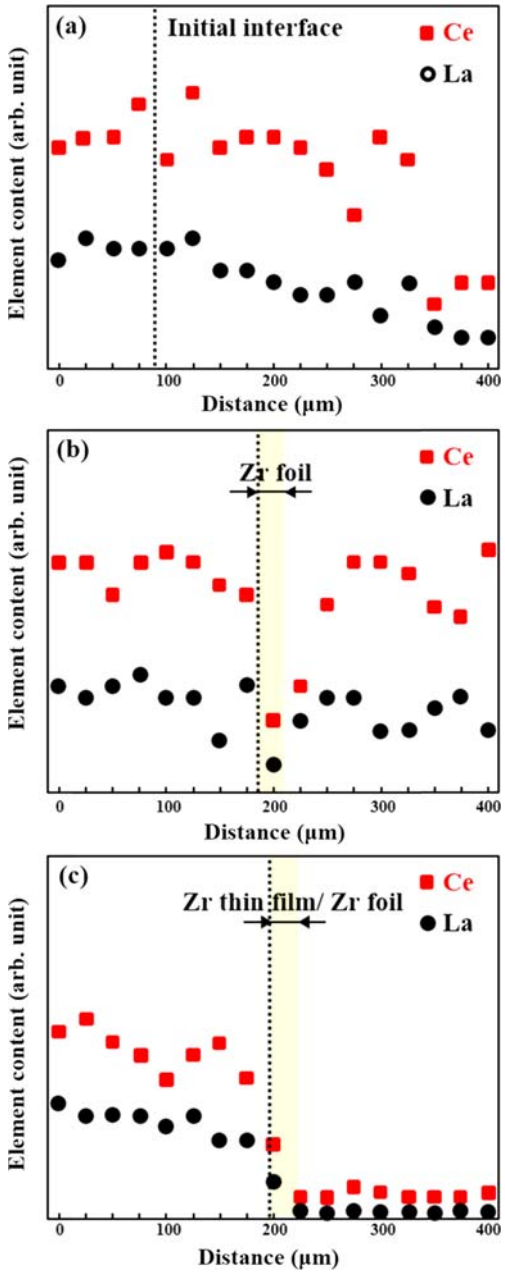

Fig. 8. Point EDS data of Ce and La content at interface of misch metal and HT9 after diffusion couple test.

To characterize each specimen and thoroughly examine the inter-diffusion behavior at the HT9/misch metal interface, the Ce and La contents were summarized by plotting the points extracted from the line EDS data. Figure 8(a) highlights bulk diffusion of Ce and La, which makes the initial interface (dashed line) indistinguishable after the diffusion couple test, as in this case there is no diffusion resistance. Figure 8(b) shows a marked decrease in the amount of Ce and La at the Zr foil region (highlighted in yellow) even though Ce and La diffused over the Zr foil barrier, with their corresponding content increasing up to almost 300 μm. As shown in Fig. 8(c), the Ce and La contents rapidly decrease at the Zr thin film/Zr foil region. Moreover, the amount of Ce and La contents is reduced with increasing diffusion length.

4. CONCLUSION

The inter-diffusion between HT9 nuclear cladding and misch metal fusion products has been studied at the SFR operating temperature. Samples of (1) misch metal/HT9, (2) misch metal/Zr foil/HT9, and (3) misch metal/Zr thin film/Zr foil/HT9 showed a different diffusion behavior. Misch metal/HT9 and misch metal/Zr foil/HT9 specimens showed inter-diffusion of Fe, Cr, Ce, and La elements. However, a misch metal/Zr thin film/Zr foil/HT9 specimen exhibited excellent performances for preventing inter-diffusion because the Zr thin film layer covered the defects present in the bare Zr foil surface. To optimize the barrier performance, Zr thin film should be investigated with various sputtering input power and pressure. These results indicate that the Zr thin film/Zr foil/HT9 system is a potential candidate for use in nuclear cladding.

ACKNOWLEDGMENTS

This research was supported by the Nuclear Research and Development Program through the National Research Foundation of Korea (NRF) funded by the Minister of Science, ICT and Future Planning (2011-0018778).

REFERENCES

1. J. Guidez, S. C. Chetal, P. Chellapandi, and B. Raj, *Nucl. Technol.* **164**, 207 (2008).

2. J. H. Kim, H. J. Ryu, J. H. Baek, S. J. Oh, B. O. Lee, C. B. Lee, and Y. S. Yoon, *J. Nucl. Mater.* **394**, 144 (2009).
3. T. Ogata, *Mater. Trans.* **44**, 47 (2003).
4. Y. I. Jung, S. H. Kim, H. G. Kim, J. Y. Park, and Y. H. Koo, *Met. Mater. Int.* **21**, 173 (2015).
5. D. W. Lim, D. J. Park, J. Y. Park, H. Jang, J. S. Yoo, Y. K. Mok, J. M Suh, and K. M. Lee, *Korean J. Met. Mater.* **52**, 493 (2014).
6. D. J. Kim, H. P. Kim, and S. S. Hwang, *Met. Mater. Int.* **20**, 1059 (2014).
7. V. Firouzdor, L. Wilson, B. Semerau, K. Sridharan, and T. R. Allen, *J. Nucl. Mater.*, **438**, 268 (2013).
8. A. B. Cohen, *Joint American Nuclear Society/European Nuclear Society International Meeting On Fifty Years of Controlled Nuclear Chain Reaction*, CONF-921102-29, Chicago, USA (1992).
9. D. D Keiser and M. C. Petri, *Annual Conference of the Canadian Nuclear Society*, CONF 940631-1, Toronto, Canada (1994).
10. J. H. Kim, J. H. Baek, B. O. Lee, C. B. Lee, and Y. S. Yoon, *Met. Mater. Int.* **17**, 535 (2011).
11. S. W. Yang, H. J. Ryu, J. H. Kim, B. O. Lee, and C. B. Lee, *J. Nucl. Mater.* **401**, 98 (2010).
12. G. W. Egeland, R. D. Mariani, T. Hartmann, D. L. Porter, S. L. Hayes, and J. R. Kennedy, *J. Nucl. Mater.* **440**, 178 (2013).
13. H. J. Ryu, B. O. Lee, S. J. Oh, J. H. Kim, and C. B. Lee, *J. Nucl. Mater.* **392**, 206 (2009).
14. D. D. Keiser Jr, and M. A. Dayananda, *J. Nucl. Mater.* **200**, 229 (1993).
15. D. D. Keiser Jr and M. C. Petri, *J. Nucl. Mater.* **240**, 51 (1996).
16. T. Ogata, M. Kurata, K. Nakamura, A. Itoh, and M. Akabori, *J. Nucl. Mater.* **250**, 171 (1997).
17. K. Nakamura, T. Ogata, M. Kurata, A. Itoh, and M. Akabori, *J. Nucl. Mater.* **275**, 246 (1999).
18. R. L. Klueh and A. T. Nelson, *J. Nucl. Mater.* **371**, 37 (2007).
19. S. H. Jee, K. S. Lee, J. H. Kim, and Y. S. Yoon, *Current Applied Physics*, **13**, 1995 (2013).
20. T. B. Massalski, J. L. Murray, L. H. Bennett, H. Baker, and L. Kacprzak, *Binary Alloy Phase Diagrams*, 2nd ed., Vol. 2, p.1051, ASM International (1986).